Available online at www.sciencedirect.com
SCIENCE DIRECT®
PERGAMON
Polyhedron 22 (2003) 1777–1782
POLYHEDRON
www.elsevier.com/locate/poly

Single-molecule magnetism behavior of $[Mn_{12}O_{12}(O_2CR)_{16}(H_2O)_4]^{2-}$ salts

Mònica Soler [a], Wolfgang Wernsdorfer [b], Khalil A. Abboud [a], David N. Hendrickson [c], George Christou [a,*]

[a] Department of Chemistry, University of Florida, Gainesville, FL 32611-7200, USA
[b] Laboratoire Louis Néel-CNRS, BP 166, Grenoble 38042, France
[c] Department of Chemistry, University of California at San Diego, La Jolla, CA 92093-0358, USA

Received 6 October 2002; accepted 8 January 2003

Abstract

$(PPh_4)_2[Mn_{12}O_{12}(O_2CCHCl_2)_{16}(H_2O)_4]$ (**3**) has been prepared by the two-electron reduction of $[Mn_{12}O_{12}(O_2CCHCl_2)_{16}(H_2O)_4]$ (**2**) using iodide. Crystallization from CH_2Cl_2/hexanes yields a mixture of two crystal forms, $\mathbf{3}\cdot 4CH_2Cl_2\cdot H_2O$ (**3a**) and $\mathbf{3}6CH_2Cl_2$ (**3b**), which are triclinic and monoclinic, respectively. They are both trapped valence 2Mn(II), 6Mn(III), 4Mn(IV). DC magnetization data for dried, unsolvated **3** in 1.80–4.00 K and 10–70 kG ranges were fit to give $S = 10$, $D = -0.28$ cm^{-1}, $g = 2.00$. Frequency-dependent out-of-phase (χ''_M) signals in AC susceptibility studies on crystalline sample of **3a** and **3b** combined with DC relaxation decay data were fit to the Arrhenius equation to give an effective energy barrier of $U_{eff} = 18.5$ and 30.3 K, respectively. Magnetization vs. DC field sweeps on single crystals of **3a** and **3b** gave hysteresis loops containing steps due to quantum tunneling of magnetization (QTM). The step separations yielded $|D|/g$ values of 0.087 and 0.14 cm^{-1}, and consequently $U = 20$ and 39 K (for $g = 2$) for **3a** and **3b**, respectively, suggesting that the differences in U_{eff} are primarily caused by changes to D. This work demonstrates the sensitivity of the magnetic properties of $[Mn_{12}]^{2-}$ single-molecule magnets to subtle differences in their environment.

Keywords: Single-molecule magnets; Magnetization; Two-electron reduction; Crystallization

1. Introduction

Single-molecule magnets (SMMs) are molecules that have a large spin ground state and large negative magnetic anisotropy due to zero-field splitting in the ground state. These properties give rise to an energy barrier for the reversal of the direction of the magnetization. The height of the barrier has an upper limit given by $(S^2|D|)$ for integer spins and $((S^2-1/4)|D|)$ for half-integer spins. When an external magnetic field is applied to an SMM, its magnetic moment becomes aligned parallel to the applied field. When the field is removed and if the temperature is low enough, the molecule retains its magnetization orientation and will only very slowly reorient.

The family of SMMs has grown considerably during the last few years. Most of the new examples have been found in manganese chemistry [1], although examples have been obtained with other metal ions such as V_4, Fe_4, Fe_8, Co_4 and Ni_{12} complexes [2]. Examples in manganese chemistry include Mn_4, Mn_{12}, Mn_{18}, Mn_{21} and Mn_{30}, but the first and the most studied example to date is $[Mn_{12}O_{12}(O_2CMe)_{16}(H_2O)_4]\cdot 4H_2O\cdot 2MeCO_2H$ (**1**) or Mn_{12}ac [3]. It possesses an $S = 10$ ground state split by axial zero-field splitting ($D = -0.50$ cm^{-1}) giving an energy barrier for the reversal of the direction of the magnetization vector. As a result, complex **1** shows slow magnetization relaxation and hysteresis in magnetization vs. field scans, being a magnet below 3 K. The observation of quantum tunneling of magnetization

* Corresponding author. Tel.: +1-352-392-8314; fax: +1-352-392-8757.
E-mail address: christou@chem.ufl.edu (G. Christou).

0277-5387/03/$ - see front matter
doi:10.1016/S0277-5387(03)00252-3

(QTM) in Mn_{12}ac [4] was also important because QTM is a fundamental process predicted theoretically, but not clearly seen before in nanoscale magnetic particles. Since the first studies on Mn_{12}ac, there has been great interest in trying to understand the phenomenon of single-molecule magnetism and particularly the magnetic properties of the family of $[Mn_{12}O_{12}(O_2CR)_{16}(H_2O)_4]$ (R = various) complexes, which display single-molecule magnetism behavior at the highest temperatures [5].

In this paper, we report the study of a two-electron reduced Mn_{12} complex, $(PPh_4)_2[Mn_{12}O_{12}(O_2CCHCl_2)_{16}(H_2O)_4]$ (**3**). It possesses an $S = 10$ ground state and retains the single-molecule magnetism properties of the Mn_{12} and $[Mn_{12}]^-$ analogues [6]. Crystallization from CH_2Cl_2/hexanes yields a mixture of two crystal forms, $\mathbf{3}\cdot 4CH_2Cl_2H_2O$ (**3a**) and $\mathbf{3}\cdot 6CH_2Cl_2$ (**3b**), both of which have been structurally characterized. The two forms have significantly different barriers to magnetization relaxation, emphasizing the influence of subtle environmental differences resulting from crystal packing (space group) symmetry and lattice solvent molecules on the resulting magnetic properties of SMMs.

2. Results and discussion

The treatment of $[Mn_{12}O_{12}(O_2CCHCl_2)_{16}(H_2O)_4]$ (**2**) with 2 equiv. of PPh_4I in MeCN gives complex **3** and I_2; the latter can be extracted from the solution mixture into a hexane phase. Subsequent removal of MeCN in vacuo and recrystallization from CH_2Cl_2/hexanes gave black crystals of $(PPh_4)_2[Mn_{12}O_{12}(O_2CCHCl_2)_{16}(H_2O)_4]$ (**3**) in good yield ($\geq 60\%$) and analytical purity (Eq. (1)).

$$[Mn_{12}O_{12}(O_2CCHCl_2)_{16}(H_2O)_4] + 2I^- \rightarrow [Mn_{12}O_{12}(O_2CCHCl_2)_{16}(H_2O)_4]^{2-} + I_2 \quad (1)$$

Recrystallization of **3** from a CH_2Cl_2/hexanes layering gives two kinds of black crystals with different morphologies, plate-like $(PPh_4)_2[Mn_{12}O_{12}(O_2CCHCl_2)_{16}(H_2O)_4]\cdot 4CH_2Cl_2\cdot H_2O$ ($\mathbf{3}\cdot 4CH_2Cl_2\cdot H_2O$ or **3a**) and needle-like $(PPh_4)_2[Mn_{12}O_{12}(O_2CCHCl_2)_{16}(H_2O)_4]\cdot 6CH_2Cl_2$ ($\mathbf{3}\cdot 6CH_2Cl_2$ or **3b**), both of which have been structurally characterized.

2.1. X-ray crystallography for $(PPh_4)_2[Mn_{12}O_{12}(O_2CCHCl_2)_{16}(H_2O)_4]\cdot 4CH_2Cl_2\cdot H_2O$ (3a) and $(PPh_4)_2[Mn_{12}O_{12}(O_2CCHCl_2)_{16}(H_2O)_4]\cdot 6CH_2Cl_2$ (3b)

Two types of crystals have been identified from the recrystallization of complex **3** in CH_2Cl_2/hexanes; the majority by far is plate-like (**3a**) and the minority is needle-like (**3b**). In some crystallization, only **3a** is apparent. Color PovRay plots of the anions of complexes **3a** and **3b** are presented in Figs. 1(a) and (b).

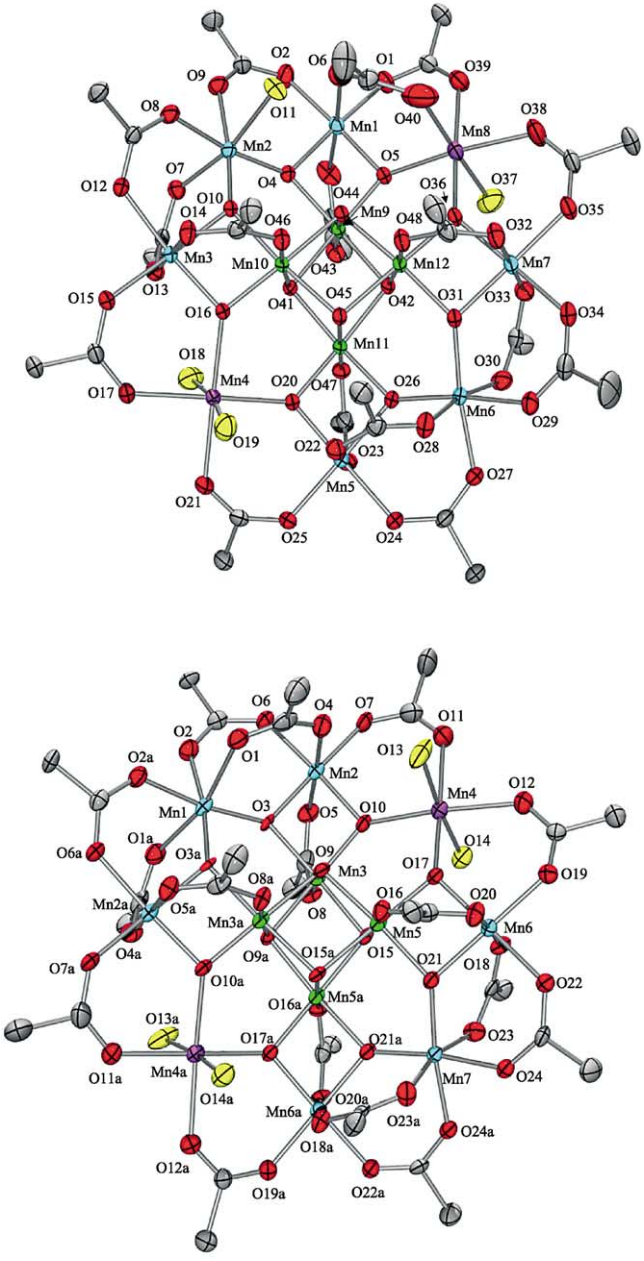

Fig. 1. PovRay plot of the anions of $(PPh_4)_2[Mn_{12}O_{12}(O_2CCHCl_2)_{16}(H_2O)_4]\cdot 4CH_2Cl_2\cdot H_2O$ (**3a**) (top) and $(PPh_4)_2[Mn_{12}O_{12}(O_2CCHCl_2)_{16}(H_2O)_4]\cdot 6CH_2Cl_2$ (**3b**) (bottom) at the 50% probability level. For clarity, the Cl atoms are omitted.

Complex **3a** crystallizes in the triclinic space group $P\bar{1}$, with two $[Mn_{12}]^{2-}$ anions in the unit cell, two PPh_4^+ cations, four CH_2Cl_2 molecules of crystallization and a water molecule. The latter is involved in hydrogen bonding with a bound H_2O ligand on the $[Mn_{12}]^{2-}$ anion (O19···O100 = 2.618 Å). The anion consists of a central $[Mn_4O_4]$ cubane surrounded by a non-planar ring of eight Mn atoms that are bridged and connected to the cubane by eight μ_3-O^{2-} ions (Fig. 1(a)). Peripheral ligation is by 16 bridging $CHCl_2CO_2^-$ and four terminal H_2O groups. The cluster is trapped

valence 2Mn(II), 6Mn(III), 4Mn(IV). The assignment of Mn(II)/Mn(III)/Mn(IV) sites is based on relative Mn–O bond distances, bond valence sum calculations and the presence of Jahn-Teller (JT) axial elongation at six Mn(III) sites. This clearly establishes that Mn(4) and Mn(8) are Mn(II) ions. There is static disorder between one carboxylate group and an adjacent water molecule, giving a mixture of two isomers, the 1:1:2 form (70%) and the 2:2 form (30%), referring to the distribution of the four H_2O molecules. Form 1:1:2 has the carboxylate bridging Mn(1) and Mn(8) with the H_2O molecule on Mn(2), and the 2:2 form has the carboxylate bridging Mn(1) and Mn(2) with the water molecule on Mn(8). The other three waters are always located on the Mn(II) ions, two on Mn(4) and the third on Mn(8).

Complex **3b** crystallizes in the monoclinic space group $P2_1/c$, with the asymmetric unit containing half $[Mn_{12}]^{2-}$ anion lying on a C_2 symmetry axis, a PPh_4^+ cation and three CH_2Cl_2 molecules of crystallization. The structure of the $[Mn_{12}]^{2-}$ anion (Fig. 1(b)) is overall very similar to that of **3a**. There is a crystallographic C_2 axis passing through Mn(2) and Mn(3). Again the cluster is trapped valence 2Mn(II), 6Mn(III), 4Mn(IV) with Mn(4) and Mn(4a) being the Mn(II) ions. No disorder in the H_2O positions was seen in this structure; the four H_2O molecules are bound in a 2:2 fashion to the Mn(II) atoms.

2.2. Magnetochemistry

2.2.1. DC magnetic susceptibility studies

Magnetization data were collected on dried powder of **3** in 10–70 kG and 1.80–4.00 K ranges, and are plotted as $M/N\mu_B$ vs. H/T in Fig. 2. Fitting of these data gave $S = 10$, $D = -0.27$ cm^{-1} $= -0.39$ K, $g = 2.00$ and a $|D|/g$ ratio of 0.14 ± 0.01. The ground state spin is thus similar to $S = 10$ or 19/2 values for the neutral Mn_{12} and monoanionic $[Mn_{12}]^-$ complexes, respectively. However, the anisotropy, as reflected in the absolute value of D, decreases as the Mn_{12} complex gets progressively reduced, which is consistent with a decrease in the Mn(III) content; JT distortions of the Mn(III) ions are the main source of the molecular anisotropy. The S (D) values obtained from reduced magnetization fittings for the three oxidation levels of the family of Mn_{12} dichloroacetate derivatives are: $[Mn_{12}]$, 10 (~ -0.45 cm^{-1}); $[Mn_{12}]^-$, 19/2 (~ -0.34 cm^{-1}); $[Mn_{12}]^{2-}$, 10 (~ -0.27 cm^{-1}). It is interesting to see that the spin value does not change on two-electron reduction and that the two-electron reduced Mn_{12} complex **3** functions also as an SMM. The calculated barrier for the dichloroacetate Mn_{12} family are: $[Mn_{12}]$, $U \sim 64$ K; $[Mn_{12}]^-$, $U \sim 44$ K; $[Mn_{12}]^{2-}$, $U \sim 39$ K [7].

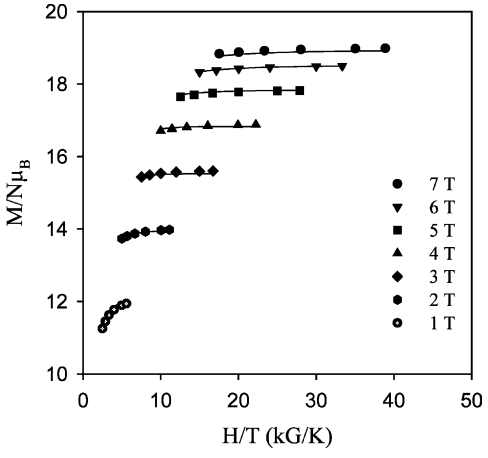

Fig. 2. Plot of $M/N\mu_B$ vs. H/T for dried complex **3** at the indicated applied fields. The solid lines are fits of the data; see the text for the fit parameters.

2.2.2. AC magnetic susceptibility studies

AC magnetic susceptibility data can be used not only to determine whether a molecule functions as an SMM but also to obtain the spin ground state (S) and the effective energy barrier U_{eff} for the magnetization relaxation. AC magnetic susceptibility studies at zero DC field and 3.5 G AC field were carried out to probe the magnetization relaxation dynamics of complex **3** at low temperatures (1.8–10 K). Fig. 3 (left) shows the in-phase (χ'_M, plotted as $\chi'_M T$ vs. T (top)) and the out-of-phase (χ''_M vs. T (bottom)) components of the AC magnetic susceptibility. If it is assumed that only the ground state of complex **3** is thermally populated in the 1.8–10 K range, the $\chi'_M T$ plateau at ~ 48 cm^3 K mol^{-1} indicates an $S = 10$ ground state with $g \sim 1.9$. In the χ''_M vs. T plot, a frequency-dependent peak is observed in the range 2–4 K at 50–1000 Hz. This also establishes that complex **3** is an SMM.

If the χ''_M signal for dried **3** at 1000 Hz in Fig. 3(a) is inspected carefully, it is apparent that it does not have a symmetric line shape and may consist of two unresolved signals. Since we knew that solvent is lost on vacuum drying, we repeated these studies with a crystalline solid that had been kept in contact with mother liquor, hoping for better resolution if more than one peak was present. Indeed, this now resulted in resolution of two χ''_M signals, shown in Fig. 3(b), and these were readily assignable to the two crystal forms of **3**. Subsequent studies using hand-picked plates of $\mathbf{3}\cdot 4CH_2Cl_2\cdot H_2O$ (**3a**) gave only the low-temperature signal, and the high-temperature signal is thus due to $\mathbf{3}\cdot 6CH_2Cl_2$ (**3b**). Bulk samples (not hand-picked) vary in their relative content of **3a** and **3b**, and thus give a variation in the relative ratio of the two χ''_M signals; in some cases, the high-temperature signal is barely visible. Resolution of the two peaks is only seen with crystals kept wet with mother liquor; removal of the mother liquor initiates solvent loss, and the peaks get progressively broader with time and merge into one broad peak.

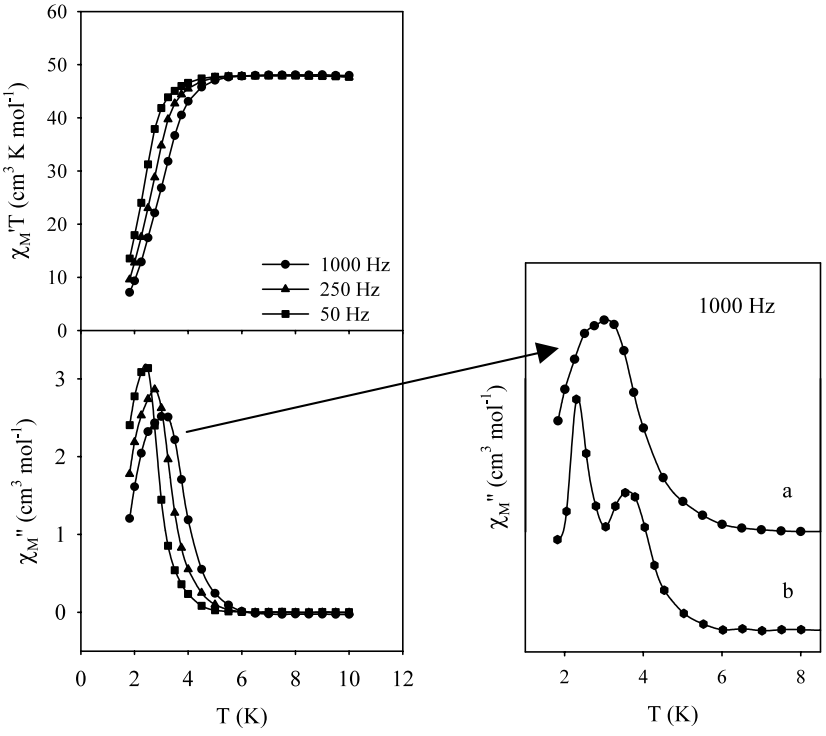

Fig. 3. Plots of the in-phase (χ'_M, plotted as $\chi'_M T$ vs. T (top)) and out-of-phase (χ''_M vs. T (bottom)) AC magnetic susceptibility for eicosane-restrained dried complex **3** (left). Out-of-phase (χ''_M) AC magnetic susceptibility plots for crystalline sample of complex **3** (right).

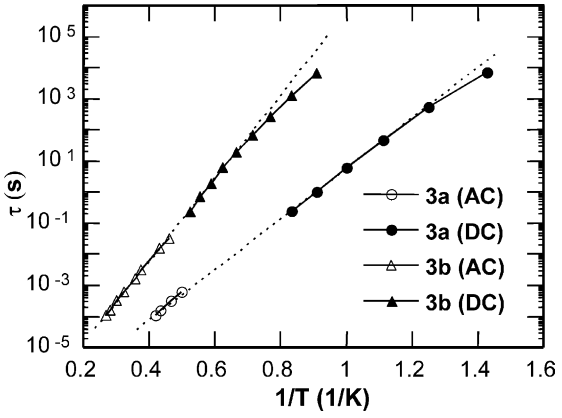

Fig. 4. Plots of relaxation time (τ) vs. $1/T$ for complexes **3a** and **3b** using AC χ''_M and DC magnetization decay data. The solid lines are fits to the Arrhenius equation; see the text for the fitting parameters.

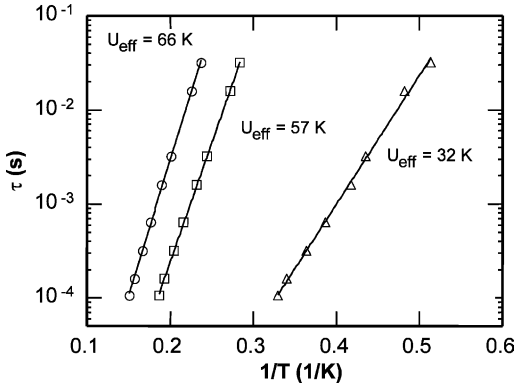

Fig. 5. Plots of relaxation time (τ) vs. $1/T$ for dried complexes $[Mn_{12}]$ (○), $[Mn_{12}]^-$ (□) and $[Mn_{12}]^{2-}$ (**3**) (△) using AC χ''_M data. The solid lines are fits to the Arrhenius equation; see the text for all the fit parameters.

For crystalline samples of **3a** and **3b**, the frequency dependence of both sets of χ''_M peaks was determined at eight different oscillation frequencies in the 5–1500 Hz range. For the low-temperature peaks, only at the four highest frequencies was a peak maximum observed, and therefore these AC data were supplemented with relaxation data at lower temperatures from DC relaxation decay measurements on single crystals of **3a** (and **3b** also) using a micro-SQUID apparatus.

The combined AC and DC relaxation data were fit to Eq. (2). The data and the fits (solid lines) are plotted as τ vs. $1/T$ in Fig. 4. For plate-like complex **3a**, $U_{eff} = 18.5$ K and the pre-exponential factor is $1/\tau_0 = 1.9 \times 10^7\ s^{-1}$. For needle-like complex **3b**, $U_{eff} = 30.3$ K and the pre-exponential factor is $1/\tau_0 = 3.1 \times 10^7\ s^{-1}$. These correspond to the low- and high-temperature peaks in Fig. 3 (right), respectively. Thus, the two crystalline forms of complex **3** have significantly different barriers to magnetization relaxation, differing by almost a factor of 2.

$$\ln\left(\frac{1}{\tau}\right) = \ln\left(\frac{1}{\tau_0}\right) - \frac{U_{eff}}{kT} \tag{2}$$

The χ''_M vs. T data for dried complex **3** were analyzed similarly using only the AC data, and compared to dried

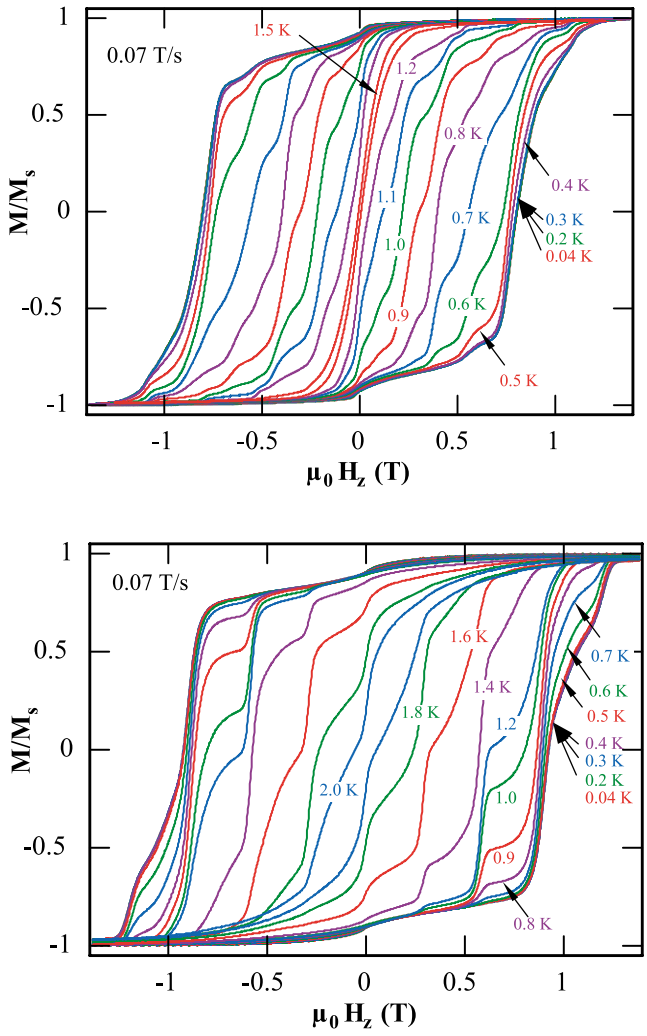

Fig. 6. Magnetization hysteresis loop for complex **3a** in 0.04–1.5 K temperature range at a 0.07 T s^{-1} field sweep rate (top). Magnetization hysteresis loop for complex **3b** in 0.04–2.0 K range at 0.07 T s^{-1} sweep rate (bottom).

samples of neutral and one-electron reduced dichloroacetate Mn_{12} derivatives. The data are shown in Fig. 5. The obtained values were: $[Mn_{12}]$, $U_{eff} = 66$ K and $1/\tau_0 = 2.0 \times 10^8$ s^{-1}; $[Mn_{12}]^-$, $U_{eff} = 57$ K and $1/\tau_0 = 5.8 \times 10^8$ s^{-1}; $[Mn_{12}]^{2-}$, $U_{eff} = 32$ K and $1/\tau_0 = 3.1 \times 10^8$ s^{-1}. The U_{eff} values decrease on reduction, as expected from the decreasing Mn(III) content mentioned earlier. The trend is monotonic but not linear, and this is as expected: the U_{eff} value depends not just on S and D, but also on the rhombic ZFS parameter E, fourth-order spin Hamiltonian parameters, the precise tunneling channel of QTM (i.e. which M_s levels are involved) and other parameters. These depend on many factors, including the site-symmetry of the complex, and the $[Mn_{12}]^{z-}$ complexes do not all crystallize in the same space group. Thus, there are too many parameters that contribute to the observed U_{eff} to permit a quantitative comparison between different complexes.

2.2.3. Hysteresis loops

Magnetization vs. DC field scans were performed on aligned single crystals of **3a** and **3b** using a micro-SQUID apparatus and the resulting hysteresis loops at temperatures <2 K and a 0.07 T s^{-1} sweep rate are shown in Fig. 6. Both **3a** and **3b** display clear hysteresis with coercivities that vary with temperature, as expected for SMMs, becoming temperature-independent only at very low temperatures (0.3 and 0.4 K for **3a** and **3b**, respectively) where crossover occurs to pure ground-state tunneling, i.e. thermally activated relaxation ceases and there is tunneling only between the lowest-lying $M_s = \pm 10$ levels. Since this crossover T is proportional to S and D, this implies that D for **3a** is less than that for **3b**. The hysteresis loops are not smooth but instead comprise plateau-like regions, which are the signature of QTM. The field separation between steps (ΔH), which can best be determined from the first derivative of the

hysteresis loop, is proportional to D. Measurement of the step positions in Fig. 6 gave an average ΔH of 0.186 T (1.86 kG) for complex **3a** (top) and 0.300 T (3.00 kG) for complex **3b** (bottom). These correspond to $|D|/g$ values of 0.087 and 0.14 cm^{-1} for **3a** and **3b**, respectively, and again indicate that the $|D|$ value for **3a** is smaller than that for **3b**, since the g values are expected to be very similar, if not identical. This is consistent with a higher energy barrier for complex **3b** due to a higher D value, being $U = S^2|D| = 25$ and 40 K for **3a** and **3b**, respectively (for $g = 2$). This parallels the difference in U_{eff} values between **3a** and **3b**, and for each crystal form, $U > U_{eff}$, as expected in the presence of QTM.

3. Conclusions

A third oxidation level of the Mn_{12} family of SMMs has been successfully isolated and studied. Complex **3** has been obtained in two crystal forms, both of which have been structurally characterized. They both have normal orientations of their JT axes, but there are distinct differences in their magnetic properties, which can be assigned to the environmental differences about the $[Mn_{12}]^{2-}$ anions resulting from the different space groups of the two forms. AC and DC susceptibility studies establish that both forms have $S = 10$ but distinctly different U_{eff} values that arise primarily from different values of the axial anisotropy parameter, D. This again emphasizes the importance of the environment and local symmetry about an SMM on the resulting magnetic properties. Both **3a** and **3b** display resonant QTM as do the Mn_{12} and $[Mn_{12}]^{-}$ analogues, and the present work thus provides another useful integer-spin system with which to study this important quantum behavior, as well as quantum phase interference [8].

Acknowledgements

This work was supported by the National Science Foundation.

References

[1] (a) S.M.J. Aubin, M.W. Wemple, D.M. Adams, H.-L. Tsai, G. Christou, D.N. Hendrickson, J. Am. Chem. Soc. 118 (1996) 7746;
(b) H. Andres, R. Basler, H.-U. Gudel, G. Aromi, G. Christou, H. Buttner, B. Ruffle, J. Am. Chem. Soc. 122 (2000) 12469;
(c) W. Wernsdorfer, N. Aliaga-Alcalde, D.N. Hendrickson, G. Christou, Nature 416 (2002) 406;
(d) G. Aromi, S. Bhaduri, P. Artus, K. Folting, G. Christou, Inorg. Chem. 41 (2002) 805;
(e) C. Boskovic, E.K. Brechin, W.E. Streib, K. Folting, J.C. Bollinger, D.N. Hendrickson, G. Christou, J. Am. Chem. Soc. 124 (2002) 3725;
(f) J.P. Price, S.R. Batten, B. Moubaraki, K.S. Murray, Chem. Commun. (2002) 762;
(g) E.K. Brechin, C. Boskovic, W. Wernsdorfer, J. Yoo, A. Yamaguchi, E.C. Sañudo, T.R. Concolino, A.L. Rheingold, H. Ishimoto, D.N. Hendrickson, G. Christou, J. Am. Chem. Soc. 124 (2002) 9710;
(h) J.T. Brockman, J.C. Huffman, G. Christou, Angew. Chem., Int. Ed. 41 (2002) 2506;
(i) M. Soler, E. Rumberger, K. Folting, D.N. Hendrickson, G. Christou, Polyhedron 20 (2001) 1365.

[2] (a) S.L. Castro, Z. Sun, C.M. Grant, J.C. Bollinger, D.N. Hendrickson, G. Christou, J. Am. Chem. Soc. 120 (1998) 2365;
(b) C. Sangregorio, T. Ohm, C. Paulsen, R. Sessoli, D. Gatteschi, Phys. Rev. Lett. 78 (1997) 4645;
(c) H. Oshio, N. Hoshino, T. Ito, J. Am. Chem. Soc. 122 (2000) 12602;
(d) A.L. Barra, A. Caneschi, A. Cornia, F. Fabrizi de Biani, D. Gatteschi, C. Sangregorio, R. Sessoli, L. Sorace, J. Am. Chem. Soc. 121 (1999) 5302;
(e) E.-C. Yang, D.N. Hendrickson, W. Wernsdorfer, M. Nakano, L.N. Zakharov, R.D. Sommer, A.L. Rheingold, M. Ledezma-Gairaud, G. Christou, J. Appl. Phys. 91 (2002) 7382;
(f) C. Cadiou, M. Murrie, C. Paulsen, V. Villar, W. Wernsdorfer, R.E.P. Winpenny, Chem. Commun. (2001) 2666.

[3] (a) R. Sessoli, H.-L. Ysai, A.R. Schake, S. Wang, J.B. Vincent, K. Folting, D. Gatteschi, G. Christou, D.N. Hendrickson, J. Am. Chem. Soc. 115 (1993) 1804;
(b) R. Sessoli, D. Gatteschi, A. Caneschi, M.A. Novak, Nature 356 (1993) 141;
(c) G. Christou, D. Gatteschi, D.N. Hendrickson, R. Sessoli, MRS Bull. 25 (2000) 66.

[4] (a) J.R. Friedman, M.P. Sarachik, J. Tejada, R. Ziolo, Phys. Rev. Lett. 76 (1996) 3830;
(b) L. Thomas, L. Lionti, R. Ballou, D. Gatteschi, R. Sessoli, B. Barbara, Nature 383 (1996) 145;
(c) J. Tejada, R.F. Ziolo, X.X. Zhang, Chem. Mater. 8 (1996) 1784.

[5] (a) H.J. Eppley, H.-L. Tsai, N. de Vries, K. Folting, G. Christou, D.N. Hendrickson, J. Am. Chem. Soc. 117 (1995) 301;
(b) S.M.J. Aubin, Z. Sun, L. Pardi, J. Krzystek, K. Folting, L.-C. Brunel, A.L. Rheingold, G. Christou, D.N. Hendrickson, Inorg. Chem. 38 (1999) 5329;
(c) M. Soler, P. Artus, K. Folting, J.C. Huffman, D.N. Hendrickson, G. Christou, Inorg. Chem. 40 (2001) 4902;
(d) P. Artus, C. Boskovic, J. Yoo, W.E. Streib, L.-C. Brunel, D.N. Hendrickson, G. Christou, Inorg. Chem. 40 (2001) 4199.

[6] (a) M. Soler, S.K. Chandra, D. Ruiz, E.R. Davidson, D.N. Hendrickson, G. Christou, Chem. Commun. (2000) 2417;
(b) M. Soler, S.K. Chandra, D. Ruiz, J.C. Huffman, D.N. Hendrickson, G. Christou, Polyhedron 20 (2001) 1279.

[7] M. Soler, W. Wernsdorfer, K.A. Abboud, J.C. Huffman, E.R. Davidson, D.N. Hendrickson, G. Christou, J. Am. Chem. Soc. 135 (2003) 3576.

[8] W. Wernsdorfer, M. Soler, G. Christou, D.N. Hendrickson, J. Appl. Phys. 91 (2002) 7164.